J. Bangladesh Acad. Sci. 50(2); 233–246: June 2026 DOI: https://doi.org/10.3329/jbas.v50i2.90655

Journal of Bangladesh Academy of Sciences

Journal homepage: http://www.bas.org.bd/publications/jbas.html

Research Article

Heavy metal contamination and ecological risk assessment in the surface water of Andharmanik river system (Hilsa sanctuary), Bangladesh

Kayes Mohammad, Adiba Mosharraf[1], Ferdousi Begum[2*], Md. Rashed Alam[3], Modhuparna Dey[4], Mohammad Moniruzzaman[5] and Md. Abu Bin Hasan Susan[6]

Department of Oceanography and Hydrography, Bangladesh Maritime University, Dhaka 1216, Bangladesh

ARTICLE INFO

Article History

Received: 29 March 2026
Revised: 22 April 2026
Accepted: 23 April 2026

Keywords: Andharmanik river, Ecological risk assessment, ECR 2023, Heavy metal contamination, Hilsa sanctuary.

ABSTRACT

Andharmanik river system (ARS), a Hilsa sanctuary on the southern coast of Bangladesh, is a critical ecological zone supporting fisheries biodiversity and local livelihoods. However, increasing anthropogenic pressures in the surrounding coastal region have heightened concerns regarding heavy metal (HM) contamination and associated ecological risks. Hence, the present study aimed to measure HM concentrations in the surface water (SW) of ARS using Inductively Coupled Plasma Mass Spectrometry method, assess the spatial distribution and evaluate their ecological risk, where samples were collected from 10 stations during the winter season of 2024 positioned by Global Positioning System (GPS). The average concentration of HMs followed the order: Zn (1.41) > Ni (0.09) > Pb (0.07) > Cr (0.052) > Cu (0.046) > Mn (0.019) > As (0.008) > Cd (0.0005) > Hg (0.00001) in mg/L; notably, Pb, As, Cr and Ni being considered as the major contaminants under the Bangladesh Environment Conservation Rules (ECR) 2023. Sources of HMs were estimated by principal component analysis (PCA) and hierarchical cluster analysis (HCA), along with Pearson correlation. Multiple indices were used to assess HM contamination status and the results showed a *low* to *moderate* contamination. The findings highlight an increasing environmental stress on this protected river system and underscore the importance of long-term monitoring and sustainable management strategies to safeguard the ecological health of ARS and its vital Hilsa habitat.

Introduction

Heavy metals (HMs) contamination in rivers and estuaries has become a major global environmental concern because of their persistence, non-biodegradability, bioaccumulation potential, and toxicity, even at low concentrations (Ali et al., 2019). HMs such as Pb, As, Cd, Cr, Cu, Hg, Mn, Ni, and Zn can emanate in the aquatic environment from both natural processes (weathering of rocks and volcanic eruptions) and anthropogenic sources (industrial effluents, ship breaking, agricultural runoff, dredging operations, and urban wastewater discharges). These sources can add HMs in aquatic ecosystems at levels that are significantly higher than the natural ambient

*Corresponding author:<ferdousi.chem@bmu.edu.bd>

[1]*Climate Change and Environment Unit, Institute of Water Modelling, Dhaka 1230, Bangladesh;* [2]*Department of Chemistry, Bangladesh Maritime University, Dhaka 1216, Bangladesh;* [3]*Department of Geography and Environment, Jahangirnagar University, Savar, Dhaka 1342, Bangladesh;* [4]*Department of Marine Fisheries and Aquaculture, Bangladesh Maritime University, Dhaka 1216, Bangladesh;* [5]*Bangladesh Council of Scientific and Industrial Research, Dhaka 1205, Bangladesh;* [6]*Department of Chemistry, University of Dhaka, Dhaka, Dhaka 1000, Bangladesh.*

concentration (Ali et al., 2019; Rakib et al., 2022; Reza and Singh, 2010). Once introduced into aquatic ecosystems, these HMs may disrupt reproductive and respiratory functions of fish, which can increase toxicity through biomagnification and bioaccumulation across the food web (Sharma et al., 2024). Thus, the monitoring of HMs pollution and associated ecological risk assessment has become an essential part of global aquatic environment management.

Composite pollution indices and methods have been widely applied to gain a better understanding of the environmental impacts caused by HM contamination. Integrated methods for assessing the status of contamination and ecological risk in aquatic systems include heavy metal pollution index (HMPI), degree of contamination (CD), comprehensive pollution index (CPI), Nemerrow pollution index (NPI), pollution load index (PLI), and the potential ecological risk index (PERI) (Ajibare et al., 2022; Hossain et al., 2024; Ogbeibu et al., 2014). These indices enable the quantification of pollution levels, identification of contaminated hotspots, and assessment of potential ecological risk from exposure to multiple HMs at a time.

Within the context of Bangladesh, situated in the Ganges-Brahmaputra-Meghna deltaic system, rivers and estuaries form the foundation of fisheries, agriculture, and navigation, yet many of these water bodies are increasingly threatened by HM pollution originating from industrial discharge, shipbreaking activities, urban runoff, and agricultural inputs (Chandra Biswas et al., 2021; Rahman et al., 2019; Rakib et al., 2022). Accordingly, an elevated level of HM pollution has been recorded in various estuarine and coastal ecosystems of Bangladesh, which prompted extensive concern over ecological health as well as food safety (Hossain et al., 2024; Rakib et al., 2022).

The Andharmanik River System (ARS), a tidal river network in the coastal belt of Patuakhali district in southern Bangladesh, is an ecologically unique aquatic habitat, resulting from the mixing of freshwater with estuarine and marine water. This river system has been declared a critical sanctuary for Hilsa shad (*Tenualosa ilisha*) to protect the juvenile (called *Jatka)* and brood species, which serves as a vital spawning and nursery ground (Ali et al., 2020; Roy et al., 2022). Hilsha, the national fish of Bangladesh, contributes significantly to fisheries sector of the country, accounting for ~10.55% of the total national fish production and providing livelihood support to millions of coastal fishers and the country produces more than 5.29 lac metric tons of Hilsa annually (DoF, 2024), representing about 60% of the global Hilsa production (Akester et al., 2024), playing a key role in the economic and cultural dimension of the country.

Despite being a critical sanctuary, anthropogenic pressures are increasingly affecting the ARS due to rapid coastal development (Asaduzzaman et al., 2025; Banik et al., 2022; Roy et al., 2022). Expansion of Payra Port (PP) and Payra Thermal Power Plant (PTPP) has intensified navigational activities, dredging operations, ship trafficking, and other infrastructural development. Additionally, this protected ecosystem faces continuous threats from human-induced disturbances, including sand mining, the establishment of brick fields along the floodplains, the disposal of municipal and market waste, and pollution from upstream catchment areas. Moreover, these activities can alter hydrodynamic processes and increase resuspension of contaminated sediments, which may introduce pollutants into the aquatic system (Nayar et al., 2004).

Although some previous studies have reported on HM contamination in the coastal and estuarine regions of Bangladesh (Hossain et al., 2024; Rakib et al., 2022), an integrated assessment with various pollution indices and multivariate statistical analysis regarding the ARS is still limited. However, such information is inadequate, especially regarding HM distribution, contamination status, and ecological risk evaluation in this critical Hilsa sanctuary. Thus, the main goal of the study is to assess the spatial distribution of HMs in surface water (SW) of the ARS based on measurement of HM concentration, identify contaminated hotspots and their potential ecological risk using several pollution indices such as HMPI, CD, CPI, NPI, PLI, and PERI. Additionally, possible sources of various HMs were also monitored using multivariate statistical techniques through principal component analysis (PCA) and hierarchical cluster analysis (HCA), along with Pearson correlation. Findings of the study would

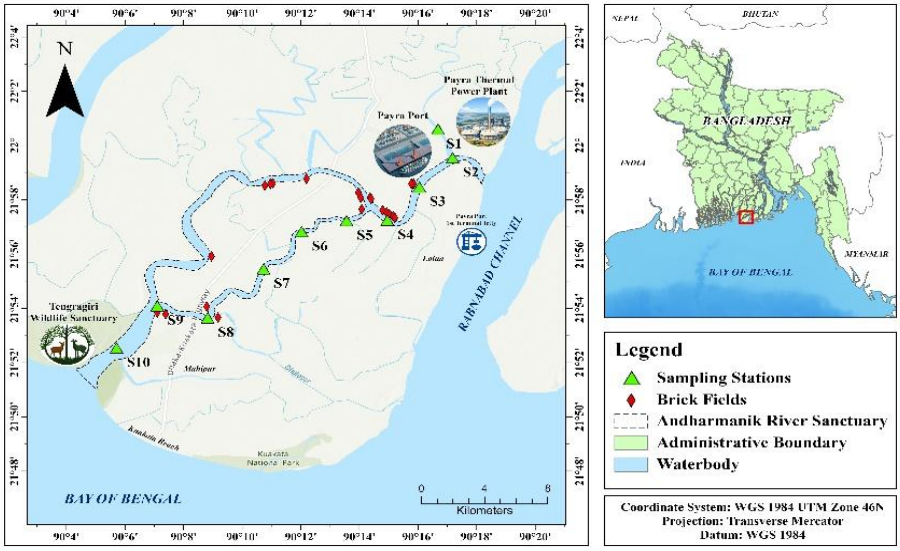

Fig. 1. Geographical coordinates of sampling stations of SW of the ARS.

enhance our understanding of the environmental status of a protected estuarine ecosystem and provide scientific evidence to implement effective monitoring and management strategies that will enable us to ensure sustainable fisheries productivity and conservation of the ARS.

Materials and Methods

Sampling site

The study was conducted in the ARS, located in Kalapara Upazila, Patuakhali district of southern Bangladesh, which is a confluence of freshwater, brackish water, and marine water. Considering the rich fish diversity and threats to the biodiversity of the ARS (Ali et al., 2020), SW were collected from 10 sampling stations at approximately 3.5 km intervals during the winter season (February 2024). Geographic location, determined by a Global Positioning System was ranged from latitude: 21°52'34.0" N to 22°00'37.7" N and longitude: 90°05'42.7" E to 90°16'40.8" E (Fig. 1). Features and structures shown on the map of the ARS are collected from satellite imagery using *Google Earth Pro* with notable surrounding features: upper stream is compacted with PP, PTPP, jetty, and multiple brick fields, indicating significant anthropogenic pressure on the ARS as well as lower stream is partially protected by a Tengragiri Wildlife Sanctuary (TWS), which helps buffer the river system from direct anthropogenic disturbances; subsequently, validation has been done during field data collection.

Sample preparation and analysis

Collected SW from the ARS was stored in 1 L acid-washed polyethylene containers. For HM analysis, 12-15 mL of SW were acidified with 1-5% HNO_3 for metal digestion that breaks down organic matter and other interfering components to keep metals in solution. PerkinElmer NexION 2000 Inductively coupled plasma-mass spectrometer (ICPMS), USA was used to measure the concentrations of HMs (Pb, As, Cd, Cr, Cu, Hg, Mn, Ni, and Zn). The nebulized material can enter Ar plasma core of the ICP-MS system at a rate of about 0.85 mL/min. The mass to charge ratio (m/z) of the HM ions produced in high-temperature plasma was measured using a quadrupole mass detector. A standard calibration curve at ppb levels was created using an ICP-multi-element standard solution XIII (Merck, Germany).

Quality assurance and quality control

Prior to standard calibration, the performance of the ICP-MS was checked by the NexION setup solution (PerkinElmer, USA). Over a dynamic range of 1 to 100 ppb, a 5-point calibration variance ($R^2 > 0.9995$) was attained. To verify the stability of the instrument, at least 3 replications were carried out. A maximum relative standard deviation (SD) of 5-8% was taken into consideration. The limits of detection (DL) and quantification (QL) were established when the response for a particular metal was 3 and 10 times higher than the background noise, respectively. To reduce errors, spike recoveries, standard reference material recoveries, and

procedure blanks were carried out as part of the quality control process.

Heavy metal contamination and ecological risk indices

Heavy metal pollution index

HMPI indicates the cumulative influence of individual HMs on SW, computed according to Hossain et al. (2024) using the equation: $HMPI = \frac{\sum_{i=1}^{n} W_i Q_i}{\sum_{i=1}^{n} W_i} \times 100$, where, Q_i and W_i are the sub-index and total weight of parameter i, respectively, and n is the number of parameters taken into account. And Q_i sub-index is calculated as $Q_i = \sum_{i=1}^{n} \frac{|M_i - I_i|}{S_i - I_i}$, where M_i, I_i, and S_i are determined as the HM concentration, desirable concentration, and recommended standard concentration of parameter i, respectively. HMPI is classified according to Table 1.

Degree of contamination

Contamination factor (CF) is a quantitative measure obtained by dividing the concentration of each HM in SW by the background value, as $CF = \frac{C_{Sample}}{C_{background}}$, where, the variable C_{sample} represents the measured concentration of the HM in SW, and $C_{background}$ represents the reference concentration, and CD was calculated by the sum of all contamination factors using the equation: $CD = \sum_{i=1}^{n} CF_i$ (Ogundele et al., 2020). Classification of CD is given in Table 1.

Pollution load index

PLI is a potential tool for HM evaluation, which was calculated as stated by Ogbeibu et al. (2014), for each site $PLI = (CF_1 \times CF_2 \times CF_3 \times ... \times CF_n)^{\frac{1}{n}}$, where n = number of HMs and CF is calculated in earlier. Indeed, PLI is characterized into two classes, given in Table 1.

Comprehensive pollution index

CPI has been employed to evaluate the status of pollution in one particular watershed based on monitoring data, computed according to Son et al. (2020) as $CPI = \frac{1}{n} \sum_{i=1}^{n} PL_{i,}$ n = number of monitoring parameters, *CD* was calculated as a sum of PL_i (the pollution index number of the i^{th} parameter). Whereas $PL_i = \frac{C_i}{S_i}$, C_i is the measured concentration of HMs, and S_i is the permitted standard concentration of HMs. CPI pollution status is categorized in Table 1.

Nemerrow's pollution index

NPI is calculated based on equations: $P_i = \frac{C_i}{S_i}$ and NPI = $\sqrt{\frac{(P_1)^2 + (max\ P_i)^2}{2}}$ according to Dey et al. (2021). Here, P_i is a pollution index of a single water quality index i, C_i for measuring the content of HMs, and S_i for the standard value of HMs. For NPI, $_{max}P_i$ = maximum value of single item pollution index at sampling point; $P_1 = \frac{1}{n} \sum_{i=1,}^{n} P_i$ is the mean value of single factor index. Detailed classification for NPI is given in Table 1.

Potential ecological risk index

PERI was calculated according to Hakanson (1980) using the mentioned equations $E_r^i = T_r^i \times C_f^i$ and $PERI = \sum_{i=1}^{n} E_r^i$, whereas C_f^i represents the CF for the i^{th} HM (calculated in earlier). E_r^i represents the ecological risk associated with a specific pollutant (i). T_r^i denotes the toxic response factor for each HM, e.g., Hg = 40, Cu = Pb = 5, As = 10, Cr = 2, Cd = 30, and Zn = 1. After the calculation, PERI is categorized as shown in Table 1.

Table 1. Classification criteria (low to high pollution) for HMPI, PLI, CPI, NPI, CD, and PERI.

Status	HMPI	Status	PLI	Status	CPI	NPI	Status	CD	PERI
Low	< 300	No Pollution	< 1.0	Sub Clean	≤ 0.40	≤ 1.0	Low	< 8	< 150
Medium	300-600	Polluted	> 1.0	Slightly Polluted	≤ 1.00	≤ 2.5	Moderate	8-16	< 300
High	> 600			Medium Polluted	≤ 2.00	≤ 7.0	Considerable	16-32	< 600
				Heavily Polluted	≥ 2.01	> 7.0	Very High	> 32	≥ 600

Multivariate statistical approach

Several multivariate statistical approaches, including descriptive statistics, Pearson correlation analysis, PCA, and HCA, were employed to gain insights into inter-relationships among the evaluated HMs contamination. All indices and descriptive statistical analyses such as mean, median, SD, standard error (SE), variance, kurtosis, and skewness, were calculated for all the measured HMs and shown with the standard value of Bangladesh Environment Conservation Rules (ECR), 2023, via *Microsoft Excel*. To evaluate the strength of the relationship among the concentration of HMs, was evaluated using the Pearson correlation, where correlation coefficients (*r*-value) and significance (*p*-value) level were estimated using *RStudio (R version 3.5.1)*. PCA and HCA have been done through *Python*, whereas PCA assists in identifying pollution sources and relationships among HMs, which transformed the original variables into principal components. HCA presented a spatial cluster pattern and contamination hotspots within the sampling site by providing valuable information for potential sources of contamination in common. Moreover, the spatial distribution pattern of calculated indices was visualized using the inverse distance weighted (IDW) method via ArcGIS Pro 3.4.0.

Results and Discussion

Heavy metal concentration in surface water of the Andharmanik river system

Fig. 2 (a-i) shows the concentration of Pb, As, Cd, Cr, Cu, Hg, Mn, Ni, and Zn in SW of the ARS and permissible limits were taken from the ECR, 2023. Concentration of Pb (Fig. 2a) displayed significant spatial variation in SW of the ARS; the highest and the lowest concentrations were recorded at S2 and S6, respectively, exceeded the ECR standard at most stations, except S3, S6, and S8. Additionally, an average concentration of Pb indicates an overall high concentration relative to the regulatory threshold (Table 2). The maximum concentration of As (Fig. 2b) was recorded at S10, situated at the opening of the Bay of Bengal (BoB), whereas the minimum was observed at S2. Unfortunately, the levels of As were consistently elevated across the ARS relative to this standard of ECR 2023, with an average value of As (Table 2). Spatial variation in the concentration of Cd of all sampling stations of the ARS was minimal (Fig. 2c), with the remaining relatively consistent. The highest value was monitored at S2, while the lowest values were at S3, S6, and S7 collectively and the average concentration of Cd was well below the regulatory limit (ECR, 2023) (Table 2). Concentration of Cr (Fig. 2d) exhibited distinct variation, with higher concentrations observed in upstream areas (S2) compared to downstream station (S8). Indeed, the average concentration slightly exceeded the permissible limit (ECR, 2023) (Table 2).

Concentrations of Cu showed limited spatial variation throughout the ARS (Fig. 2e); the highest and lowest concentrations were found at S2 and S1, respectively whereas the average concentration was substantially below the threshold limit of ECR, 2023. Hg levels showed no marked spatial variation; the maximum value was observed at S5 and the minimum at S1 (Fig. 2f), however, average concentration was below the permissible limit of ECR, 2023 (Table 2). The highest concentration of Mn (Fig. 2g) was noted at S2, while the lowest was at S9 and the average concentration across all the sampling stations of the ARS was markedly below the permissible limit of ECR, 2023 (Table 2). Concentrations of Ni showed significant spatial variation (Fig. 2h); the highest was recorded at S1 and the lowest at S8 as well as the most stations exceeded the permissible limit of ECR, 2023, except S6 and S8. Average concentration indicated an elevation above the standard (Table 2). The maximum concentration of Zn was observed at S2, while the minimum was at S9, located at the downstream channel (Fig. 2i) and the average concentration was remaining below the permissible limit of ECR, 2023 (Table 2).

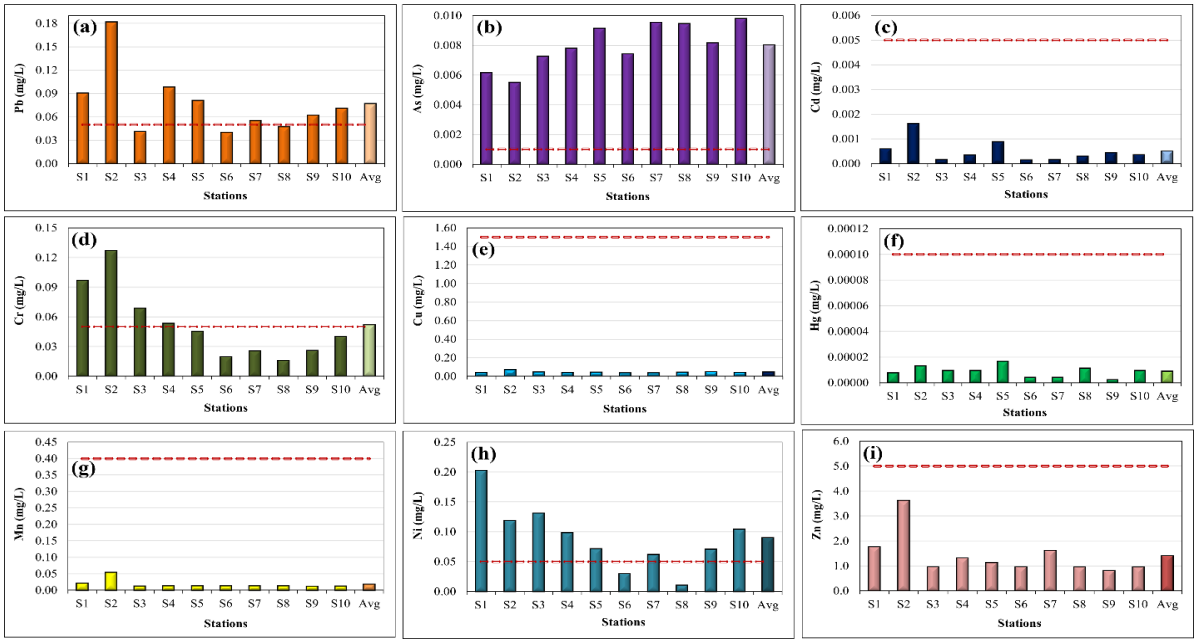

Fig. 2. Concentration of HMs in SW of the ARS with their permissible limit indicated by *red* dashed lines (ECR 2023); (a) Pb, (b) As, (c) Cd, (d) Cr, (e) Cu, (f) Hg, (g) Mn, (h) Ni, and (i) Zn.

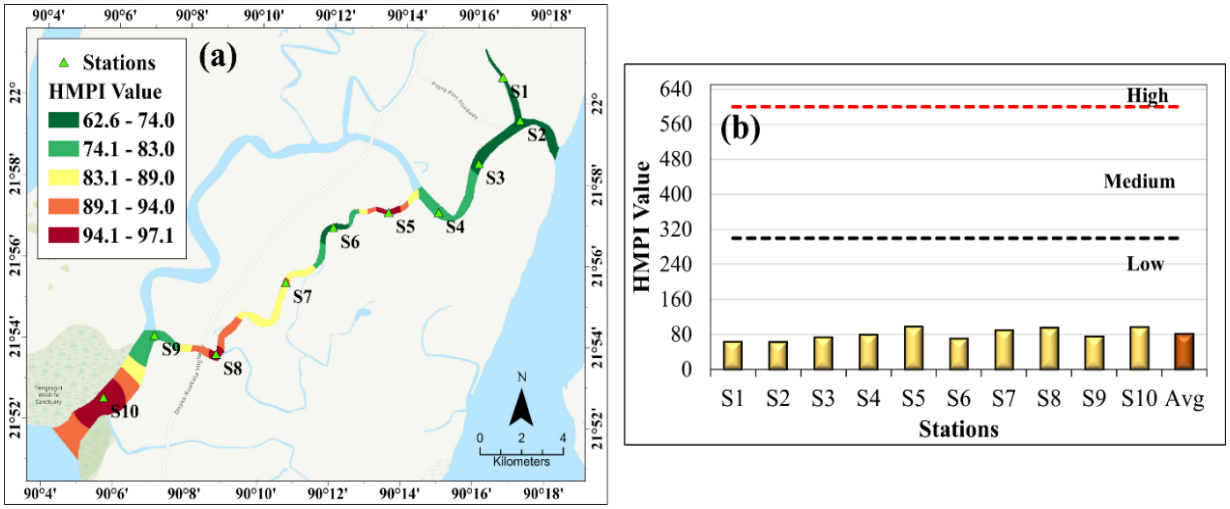

Fig. 3. (a) Spatial distribution of HMPI and (b) HMPI values for each sampling station of the ARS.

Assessment of heavy metal contamination and ecological risk

Heavy metal pollution index

Evaluation of HMPI (Fig. 3) reveals a consistently *low* pollution with the average value of 80.1 throughout SW of the ARS, indicating overall environmental quality remains within safe limits. Peak value of HMPI (~98) was observed at S5, followed closely by S10 and S8; all these stations were found near multiple brick fields (Fig. 1). Conversely, most favorable conditions were identified at S1 and S2, which yielded a minimum HMPI of ~65 suggesting that HM contamination is currently not a localized or systemic threat in SW of the ARS.

Degree of contamination

Calculated values of CD (Fig. 4) show a consistent state of *moderate* contamination in SW across the stations in the ARS, where S1, S2, and S10 indicate higher levels of contamination. Specifically, S2 near the PP and PTPP (Fig. 1) recorded the peak value of CD (~15.5), reflecting the highest cumulative impact. Whereas S6 showed the lowest level among the sampling stations, yet within the *moderate* threshold, having a value of ~9.5. On average, SW of the ARS maintains a CD of ~13, positioning the overall study sites at upper boundary of the *moderate* contamination category.

Pollution load index

PLI analysis exhibits a status of *no* to *near* pollution, characterized by a significant correlation between total metal loading and potential toxicity (Fig. 5). PLI values across most of the stations (S1 and S3-S10) remain consistently at 0.99 to 1.00, placing them exactly at the threshold between a *non-polluted* and a *polluted* status in the spatial distribution scenario. While S2 shows a marginally lower PLI of ~0.95, average PLI of 0.99 indicates the environment is on the verge of baseline degradation.

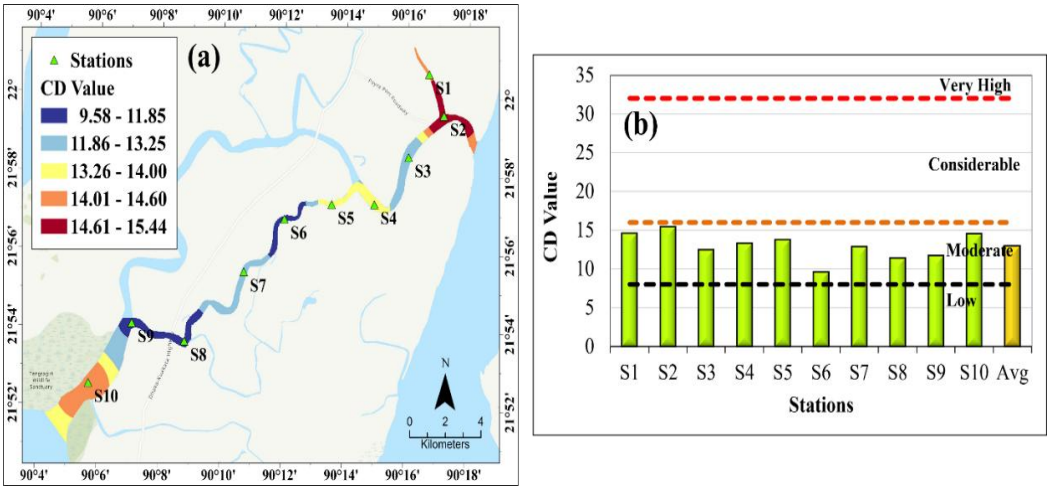

Fig. 4. (a) Spatial distribution of CD and (b) CD values for each sampling station of the ARS.

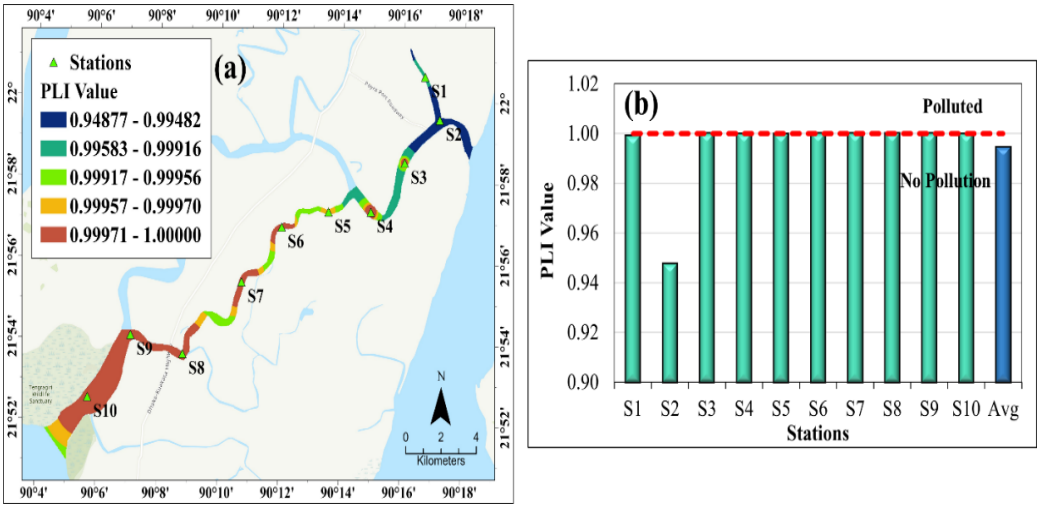

Fig. 5. (a) Spatial distribution of PLI and (b) PLI values for each sampling station of the ARS.

Comprehensive pollution index

Evaluated CPI indicates that SW of the ARS is predominantly characterized by a *medium-polluted* status since every station exceeds the baseline threshold of 1.0 (Fig. 6). Indeed, S2 and S1 exhibit the highest level of pollution which might be due to the influence of PP and PTPP operations (Fig. 1) with a CPI of 1.72 and 1.62, followed by S10 (1.62) might be as a result of accumulation HMs due to tidal and marine influence from the BoB, enhances sediment re-suspension, and particle trapping (Nayar et al., 2004). Conversely, S6 demonstrates the highest relative environmental quality, recording a minimum CPI of 1.06 and the remaining stations (S3 through S9) fluctuate between 1.27 and 1.53, culminating in a regional average CPI of 1.44 (Fig. 6). While these values remain safely below the *heavy pollution* category, uniform elevation above the slight pollution threshold indicates widespread anthropogenic influence that suggests continued monitoring to prevent further degradation (Ali et al., 2020).

Nemerrow's pollution index

Calculated NPI (Fig. 7) reveals that SW of the ARS falls within the *medium-polluted* threshold and fluctuated between 4.1 at S2 and 7.0 at S10 with notable peaks at S5, S7, and S8. The higher NPI values were noted for the downstream of the ARS, might be for deposition of HMs due to tidal influence from the BoB enhancing sediment re-suspension, and particle trapping (Nayar et al., 2004), the effects of multiple brick fields around these stations (Fig. 1). However, pollution remains consistently above the *slightly polluted* status (NPI = 2.5); no station manages to break into the *heavily polluted* zone. Ultimately, average NPI with ~5.8, confirming a stabilized *medium-polluted* condition across the geographical span of the ARS.

Potential ecological risk index

Calculated PERI of SW indicates a *moderate ecological risk* with average value of 236 at all sampling stations of the ARS (Fig. 8). Whereas PERI consistently stay above the *low ecological risk* threshold of 150 however remain below the *considerable ecological risk* of 300; a minimum of ~200 (S2 and S6) to a peak of ~285 (S10) near TWS. This substantial safety margin suggests that current concentration of HMs pose a *moderate ecological risk* to the ecosystem, especially concerning the TWS and the Hilsha sanctuary, indicating the need for long-term monitoring efforts to conserve these sanctuaries (Ali et al., 2020; Islam et al., 2020).

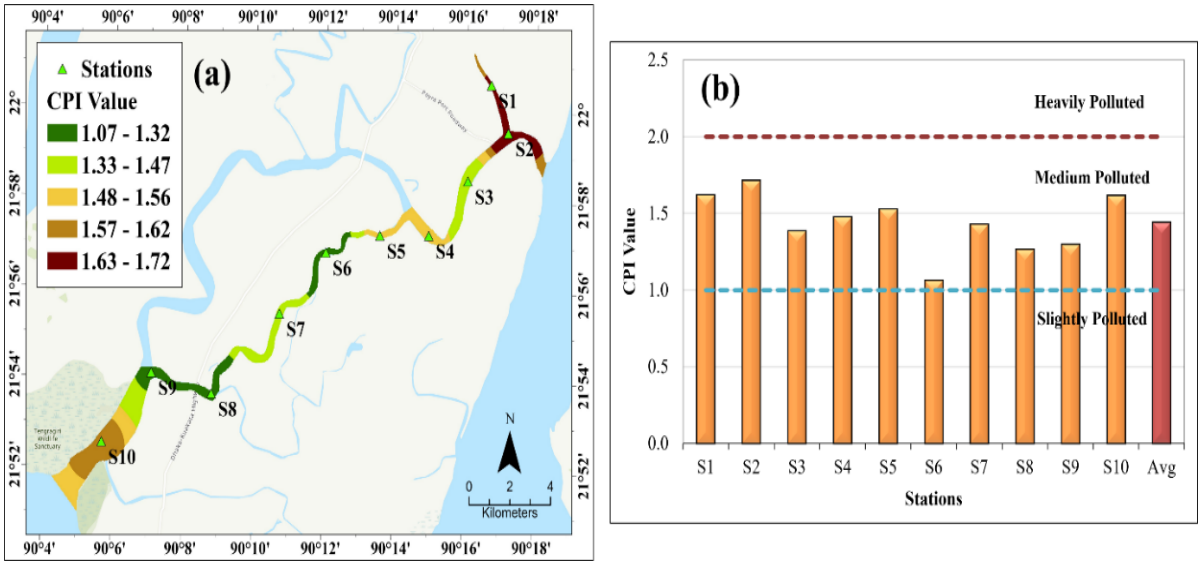

Fig. 6. (a) Spatial distribution of CPI and (b) CPI values for each sampling station of the ARS.

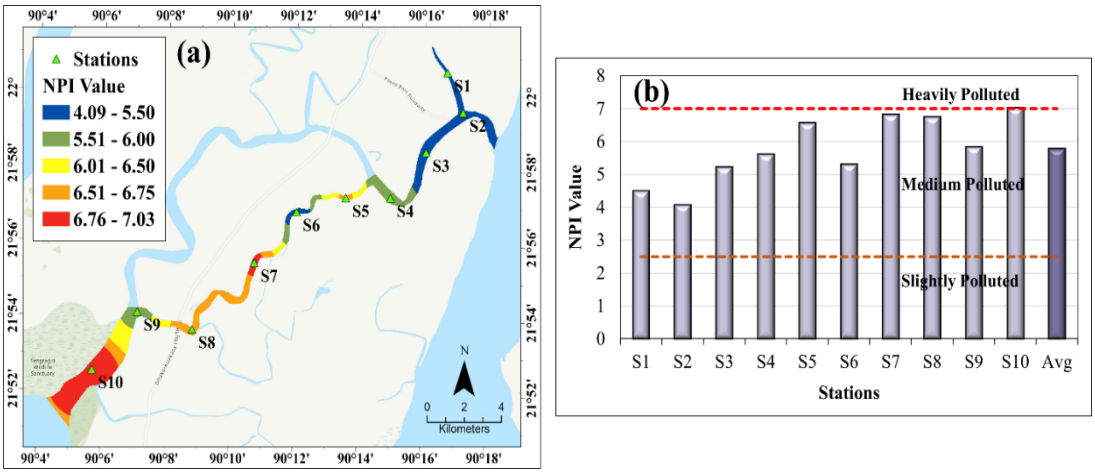

Fig. 7. (a) Spatial distribution of NPI and (b) NPI values for each sampling station of the ARS.

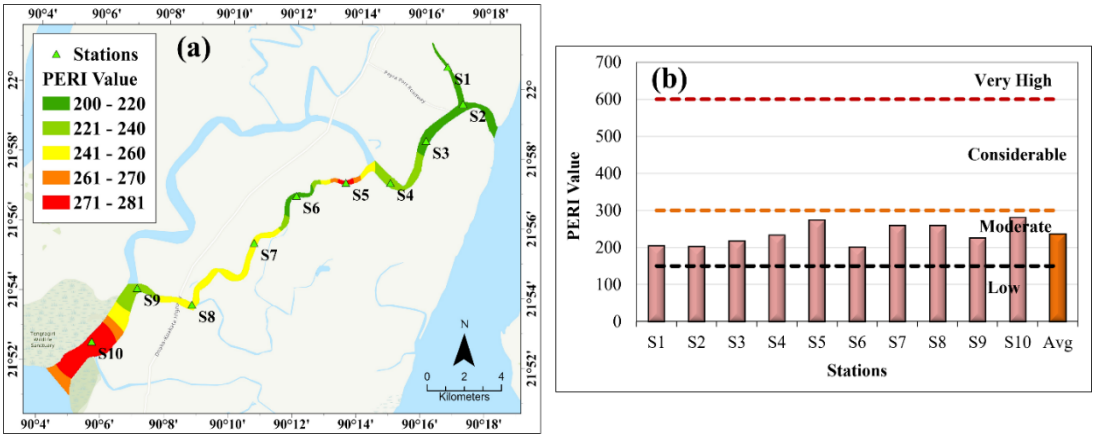

Fig. 8. (a) Spatial distribution of PERI and (b) PERI values for each sampling station of the ARS.

Multivariate analysis

Descriptive statistical analysis

Statistical analysis of measured concentration of HMs in SW of the ARS represented distinct patterns of contamination and variability (Table 2). Pb exhibited the highest exceedance, with a maximum concentration of 0.182 mg/L and an average of 0.077 mg/L, substantially surpassing the ECR 2023 permissible limit of 0.05 mg/L; the positive skewness (1.94) and elevated kurtosis (4.49) indicate a right-tailed distribution driven by several high-concentration hotspots.

Concentration of As showed consistently elevated levels (average 0.008 mg/L) compared to the standard of 0.001 mg/L, although values remained relatively uniform (low SD of 0.001 mg/L and near-symmetric distribution). Concentration of Cd were very low (average 0.0005 mg/L), well below the 0.005 mg/L limit, despite moderate positive skewness. Levels of Cr displayed a moderate average of 0.052 mg/L, slightly exceeding the 0.05 mg/L threshold, with noticeable spatial variability (SD = 0.036 mg/L). Concentration of Cu, Hg, and Mn remained far below their respective permissible limits (1.5, 0.0001, and 0.4 mg/L), with averages of 0.046, 0.00001, and 0.019 mg/L, respectively, and generally *low* variability. With an average concentration of 0.090 mg/L, almost twice the 0.05 mg/L threshold, and a maximum of 0.203 mg/L, indicating widespread exceedance, Ni posed serious concerns. Zn showed the highest

concentrations (maximum 3.623 mg/L), yet the average of 1.413 mg/L stayed comfortably below the 5 mg/L guideline. Overall, Pb, As, Cr, and particularly Ni create the primary contaminants of concern in SW of the ARS, while Cd, Cu, Hg, Mn, and Zn comply with regulatory standards, highlighting the need for targeted source identification and mitigation measures in areas of elevated metal loading.

Pearson correlation

Pearson correlation matrix in Fig. 9 reveals a complex geochemical relationship among the HMs, characterized by several highly significant positive associations and distinct inverse behaviors. Notably, Pb, Cd, Cr, Cu, and Mn showed a strong positive and significant correlation with Zn ($r \geq 0.80$, $p \leq 0.05$), suggesting these HMs share common anthropogenic or geological origins and similar transport mechanisms in the environment. Conversely, As acts as an outlier, displaying consistent negative correlations with nearly all other HMs, mostly significant with Cr ($r = -0.81$, $p \leq 0.05$) and Mn ($r = -0.69$, $p \leq 0.05$), which implies a different source or unique depositional conditions for As compared to the Pb-Cd-Cr-Cu-Mn-Zn group. Meanwhile, Hg and Ni showed less significant and more variable correlation with almost all other HMs except Ni and Cr ($r = 0.781$, $p \leq 0.05$), suggesting their presence is likely governed by independent localized factors or distinct anthropogenic activities.

Table 2. Descriptive statistics of concentration of HMs in SW of the ARS and their comparison with the permissible limits of ECR 2023.

HMs (mg/L)	Max.	Min.	Mean	Median	SD	SE	Variance	Kurtosis	Skewness	Standard (mg/L) (ECR 2023)
Pb	0.182	0.040	0.077	0.07	0.042	0.01	0.0018	4.49	1.94	0.050
As	0.010	0.006	0.008	0.008	0.001	0.00047	0.000002	-0.94	-0.423	0.001
Cd	0.0016	0.0002	0.0005	0.00036	0.0005	0.00014	0.0000002	4.03	4.95	0.005
Cr	0.127	0.016	0.052	0.043	0.036	0.011	0.001315	0.68	1.17	0.050
Cu	0.072	0.038	0.046	0.0435	0.01	0.0032	0.0001	6.96	2.48	1.500
Hg	0.00002	0.000002	0.00001	0.000010	0.000004	0.000001	0.00000000002	-0.33	0.19	0.0001
Mn	0.054	0.013	0.019	0.014	0.013	0.0041	0.000165	8.79	2.93	0.400
Ni	0.203	0.011	0.090	0.085	0.055	0.017	0.003	0.99	0.66	0.050
Zn	3.623	0.815	1.413	1.05	0.837	0.264	0.70	6.40	2.43	5.000

Source analysis of contamination by heavy metals

Principal component analysis

PCA biplot (Fig. 10a) provides a high-resolution clarification of the geochemical relationships, with the first two principal components accounting for a substantial 83.6% of the total variance. PC1, which explains 68.7% of the variance, is largely defined by the strong positive influence of HMs, such as Zn, Mn, Pb, Cu, and Cd, whose red vectors cluster closely together, reinforcing the high positive correlations observed in the raw data. Conversely, as vector points in the opposite direction along the PC1 axis, it visually confirms its inverse relationship with the other HMs. However, Ni shows positive loadings on both PC1 and PC2, indicating its contribution to the variability represented by these components and a moderate association with HMs loading positively on PC1, whereas Hg exhibits a strong negative loading on PC2 with moderate positive loading on PC1, suggesting a distinct distribution pattern likely influenced by different environmental or geochemical processes. Spatial distribution of the sampling stations within this biplot reveals three distinct environmental profiles: Cluster 1 (*blue*), comprising S6, S7, S8, and S9, is characterized by overall lower concentrations of HMs and a primary association with As influence; Cluster 2 (*green*), which includes S1, S3, S4, S5, and S10, represents areas with moderate contamination levels; and Cluster 3 (orange), where S2 is situated in the conjugation of PP and PTPP (Fig. 1) stands alone as a significant contamination hotspot, clearly exhibiting the highest levels of Pb, Zn, and Mn. According to Fig. 1, Cluster 1 is comparatively surrounded by less industrial pressure, whereas Cluster 2 (except S10) has the most pressure of PP, PTPP, and several brick field activities. Thus, the PCA analysis reveals that coastal development and anthropogenic activities like port and thermal plant operations, brick fields, and other ongoing activities have a direct influence on HM contamination at the sampling site (Fig. 1).

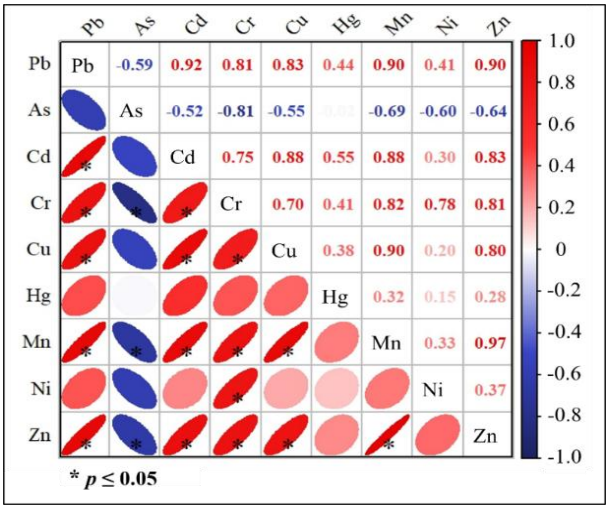

Fig. 9. Pearson correlation matrix among concentrations of HMs in SW of the ARS ($p \leq 0.05$); *Blue* indicates a *negative*, while *red* shows a *positive* correlation.

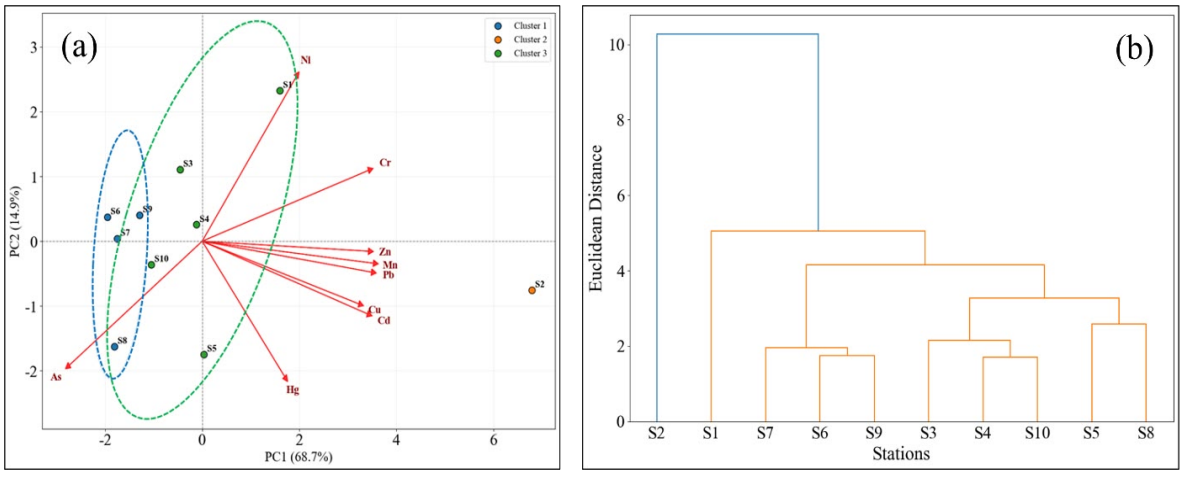

Fig. 10. (a) PCA biplot and (b) HCA of measured HMs concentration in SW of the ARS.

Hierarchical cluster analysis

Fig. 10 (b) (dendrogram) illustrates an HCA of ten sampling stations of SW of the ARS based on their Euclidean distance, which serves as a measure of similarity. Most striking feature of the dendrogram is the clear isolation of S2, which joins the remaining stations at a markedly high Euclidean distance (>10), indicating its distinct characteristics that are likely influenced by nearby PP operations and PTPP activities (Fig. 1). Remaining stations form two primary sub-clusters: a smaller group consisting of S1, S7, S6, and S9, and a larger, more tightly knit group containing S3, S4, S10, S5, and S8. Within these groups, pairs like S4 and S10 or S6 and S9 show the lowest vertical linkage heights (around 2), indicating they share the most similar profiles among all the stations analysed.

Conclusions

The Andharmanik River System, an ecologically important Hilsa sanctuary in coastal Bangladesh, is essential for the local, socio-economic, and ecological balance. It sustains biodiversity by providing fishermen a means of subsistence and essential resources. However, the ARS is currently facing serious concerns of environmental degradation due to anthropogenic pollution from Payra Port (PP), Payra Thermal Power Plant, and other coastal activities. The present study provides a comprehensive assessment of heavy metal (HM) contamination and associated ecological risks in the surface water of the ARS. The findings highlight a significant spatial variability of HMs with the decreasing order of average concentration in mg/L as Zn > Ni > Pb > Cr > Cu > Mn > As > Cd > Hg. Particularly, Pb, As, Cr, and Ni were identified as the key contaminants, where the average concentration exceeds the permissible limits of Bangladesh Environment Conservation Rules 2023. These results reflected the growing anthropogenic activities due to rapid coastal development. Moreover, calculated multiple pollution indices provided the contamination status in SW of the ARS, where the average heavy metal pollution index (HMPI = 80.1) indicated an overall *low pollution* and degree of contamination (CD = ~13), along with comprehensive pollution index (CPI = 1.44) and Nemerrow pollution index (NPI = 5.8), which suggested *moderate contamination.* Further-more, pollution load index (PLI = 0.99) values close to unity indicated the transition of SW from *unpolluted* to *polluted* conditions though the potential ecological risk index (PERI = 236) classified the ARS within a *moderate ecological risk* category. Multivariate statistical analysis indicated strong *positive* correlations among Pb, Cd, Cr, Cu, Mn, and Zn suggesting common sources or similar transport mechanisms, likely associated with anthropogenic activities. Additionally, principal component analysis marked that most HMs are influenced by human-induced inputs through port activities, dredging operations, brick fields, and other infrastructural developments in the Payra estuarine region. Hierarchical cluster analysis further identified station S2 as a distinct contamination hotspot, most likely influenced by the proximity of PP and PTPP operations, and intensified ongoing activities. However, the present contamination level remains *moderate*; the overall ecological risk assessment indicates that continued accumulation of certain HMs may pose significant ecological threats to aquatic biodiversity and fisheries sustainability in the future. Therefore, strengthening environmental monitoring programs, controlling pollutant discharge, and implementing integrated coastal management strategies are essential to safeguard the ecological integrity of the ARS.

Acknowledgment

The authors are thankful to the Bangladesh Council of Scientific and Industrial Research and the Chemistry and Chemical Oceanography Laboratory, Bangladesh Maritime University, for laboratory facilities and research support. The corresponding author also acknowledges the University Grants Commission of Bangladesh for financial support to carry out this research. Special thanks to the Payra Port Authority for their assistance during sample collection.

Authors contribution

Kayes Mohammad: Conceptualization, Data curation, Formal analysis, Methodology, Software, Validation,

Visualization, Investigation, Writing-original draft; Adiba Mosharraf: Conceptualization, Software, Validation, Visualization, Investigation, Writing-original draft; Ferdousi Begum: Supervision, Conceptualization, Data curation, Methodology, Investigation, Validation, Writing-review and editing; Md. Rashed Alam: Software, Validation, Visualization, Writing-review and editing; Modhuparna Dey: Writing-original draft; Mohammad Moniruzzaman: Formal analysis, Validation; Md. Abu Bin Hasan Susan: Writing-review and editing.

Conflict of interest

The authors declare that they have no conflict of interest regarding the publication of this article.

References

Ajibare AO, Ogungbile PO, and Ayeku PO. Evaluation of water pollution monitoring for heavy metal contamination: A case study of agodi reservoir, Oyo State, Nigeria. *Environ. Monit. Assess.* 2022, 194(10): 675.

Akester M, Bladon A, and Conallin J. Research for development: Evidence-based Hilsa management improvements in Myanmar. *Front. Mar. Sci*. 2024; 11: 1–9.

Ali H, Khan E, and Ilahi I. Environmental chemistry and ecotoxicology of hazardous heavy metals: Environmental persistence, toxicity, and bioaccumulation. *J. Chem.*, 2019; 2019(4):1–14.

Ali MM, Ali ML, Rahman MJ, and Wahab MA. Fish diversity in the andharmanik river sanctuary in Bangladesh. *Croat. J. Fish.*, 2020; 78(1): 21–32.

Asaduzzaman M, Hayder MA, Hosen MR, Rahman S, Sifa NJ, Rahman M, and Alam MK. Environmental and socio-economic impacts of coal-fired payra thermal power plant. *Bangladesh J. Phys.*, 2025; 32(1): 1–12.

Banik P, Hossain MB, Nur AAU, Choudhury TR, Liba SI, Yu J, Noman MA, and Sun J. Microplastics in sediment of Kuakata beach, Bangladesh: Occurrence, spatial distribution, and risk assessment. *Front. Mar. Sci.* 2022; 9: 1–13.

Chandra BJ, Mozammel HM, Maniruzzaman M, Akhtar S, and Kalra N. Coastal and marine pollution in Bangladesh: Pathways, hotspots and adaptation strategies. *EJ-GEO*, 2021; 2(4): 26–34.

Department of Fisheries (DOF). Yearbook of Fisheries Statistics of Bangladesh, 2023-24. Fisheries Resources Survey System (FRSS), Ministry of Fisheries and Livestock, 2024; 41: p. 140.

Dey M, Akter A, Islam S, Dey SC, Choudhury TR, Fatema KJ, and Begum, BA. Assessment of contamination level, pollution risk and source apportionment of heavy metals in the Halda river Water, Bangladesh. *Heliyon*, 2021; 7(12): 1–12.

Environmental Conservation Rules, (ECR). Ministry of Environment, Forest and Climate Change. Government of Bangladesh, 2023.

Hakanson L. An ecological risk index for aquatic pollution control - A sedimentological approach. *Water Res.*, 1980; 14(8): 975–1001.

Hossain I, Ahmed MK, Chowdhury KMA, Moniruzzaman M, and Shampa MTA. Ecological risk assessment of oil and grease (OG) and heavy metals in the surface water of Naf river, Bangladesh. *Heliyon*, 2024; 10(9): 1–20.

Islam MM, Chowdhury RM, Zaman AKMM, Rahman MS, Islam MN, Rudra AK, and Azad MS. Spatiotemporal mapping mangroves of tengragiri wildlife sanctuary under Barguna District of Bangladesh using freely available satellite imagery. *Model. Earth Syst. Env.* 2020; 6(2): 917–927.

Nayar S, Goh BPL, and Chou, L. M. Environmental impact of heavy metals from dredged and resuspended sediments on phytoplankton and bacteria assessed in in- situ mesocosms. *Ecotoxicol. Environ. Saf.* 2004; 59(3): 349–369.

Ogbeibu AE, Omoigberale, MO, Ezenwa IM, Eziza JO, and Igwe JO. Using pollution load index and geoaccumulation index for the assessment of heavy metal pollution and sediment quality of the Benin river, Nigeria. *Nat. Env.*, 2014; 2(1): 1–9.

Ogundele LT, Ayeku PO, Adebayo AS, Olufemi AP, and Adejoro IA. Pollution indices and potential ecological

risks of heavy metals in the soil: A case study of municipal wastes site in Ondo State, Southwestern, Nigeria. *Polytech.* 2020; 3(1): 78–86.

Rahman MM, Ghosh T, Salehin M, Ghosh A, Haque A, Hossain MA, Das S, Hazra S, Islam N, Sarker M H, Nicholls RJ, and Hutton CW. Ganges-Brahmaputra-Meghna Delta, Bangladesh and India: A Transnational Mega-Delta. *Deltas in the Anthropocene*, 2019; 23–51.

Rakib MRJ, Rahman MA, Onyena AP, Kumar R, Sarker A, Hossain MB, Islam ARMT, Islam MS, Rahman MM, Jolly YN, Idris AM, Ali MM, Bilal M, and Sun X. A Comprehensive review of heavy metal pollution in the coastal areas of Bangladesh: Abundance, bioaccumulation, health implications, and challenges. *Environ. Sci. Pollut. Res.* 2022; 29(45): 67532–67558.

Reza R and Singh G. Heavy metal contamination and its indexing approach for river water. *Int. J. Environ. Sci. Technol.*, 2010; 7(4): 785–792.

Roy D, Didar NB, Sarker S, Rahman KMA, and Latifa GA. Appraisal of different attributes of fish community in andharmanik river of coastal Bangladesh and socio-economic conditions of fishermen. *Heliyon*, 2022; 8(7): e09825.

Sharma M, Kant R, Sharma AK, and Sharma AK. Exploring the impact of heavy metals toxicity in the aquatic ecosystem. *IJEWR*, 2024; 9(1): 267–280.

Son CT, Giang NTH., Thao TP, Nui NH, Lam NT, and Cong VH. Assessment of Cau river water quality assessment using a combination of water quality and pollution indices. *J. Water Supply: Res. Technol. Aqua*. 2020; 69(2): 160–172.